International Journal of Heat and Mass Transfer 52 (2009) 4117–4124

Contents lists available at ScienceDirect

International Journal of Heat and Mass Transfer

journal homepage: www.elsevier.com/locate/ijhmt

Turbulent momentum transport and kinetic energy production in plane-channel flows

E.-S. Zanoun [a], F. Durst [b,*]

[a] Department of Aerodynamics and Fluid Mechanics (LAS), BTU Cottbus Siemens-Halske-Ring 14, D-03046 Cottbus, Germany
[b] FMP Technology GmbH, Am Weichselgarten 34, D-91058 Erlangen, Germany

ARTICLE INFO

Article history:
Received 19 December 2008
Accepted 23 March 2009
Available online 25 May 2009

Keywords:
Channel flow
Momentum transport
Energy production

ABSTRACT

Based on a momentum balance analysis, this paper basically presents and discusses experimental results from fully developed turbulent plane-channel flows utilizing hot-wire anemometer. The paper stresses the fact that in experimental investigations of two-dimensional shear flows it is difficult to obtain, with reasonable accuracy, all turbulent quantities of interest to fluid mechanics researchers. This makes it necessary to measure some relevant turbulent flow properties as a basis to drive others by utilizing theoretically derived relationships obtained from the mean momentum equation. It is demonstrated that both the turbulent Reynolds shear stress $(-\rho\overline{u_1' u_2'})$ and the kinetic energy production $[-\rho\overline{u_1' u_2'}(d\overline{U}/dy)]$ for two-dimensional fully developed turbulent flows can be predicted in this way through detailed mean velocity and mean pressure gradient measurements. In addition, some flow similarities and differences among channel, pipe and boundary layer flows are discussed, revealing effects of flow geometry and Reynolds number on the mean flow scaling.

© 2009 Elsevier Ltd. All rights reserved.

1. Introduction

At high Reynolds numbers, it is difficult numerically to resolve the small scales of turbulence. The same difficulties arise in experimental investigations, since the size of most of the measuring sensors are not small enough to resolve the small scales of the flow. Hence, it has become general practice to apply combined numerical and experimental techniques, supported by analytical methods, to investigate, reliably, high Reynolds number turbulent shear flows. Such combined approaches turn out to be most successful when a certain property of a turbulent flow is the aim of an investigation. Because of this, the authors have adopted the same approach, investigating two-dimensional fully developed turbulent plane-channel flows, particularly, the momentum transport and the kinetic energy production.

Recently, such two-dimensional flows were intensively investigated, see, e.g., [1–8] to obtain information on the structure of the flow field. The experimental study of Laufer [9] was among the most earliest experimental studies of such flows. Further investigations by Comte-Bellot [10], Clark [11], Eckelmann [12], Hussain and Reynolds [13], Dean and Bradshaw [14], Gad-el-Hak and Bandyopadhyay [15], Durst et al. [16], Sahay and Sreenivasan [17] and Monkwetiz and Nagib [18] were also carried out with the aim of investigating Reynolds number effect on the mean flow properties of two-dimensional channel and pipe flows. Among the most theoretically oriented work, it is worth mentioning the work of Millikan [19], Afzal and Yajnik [20], Panton [21,22], Wosnik et al. [23], and Oberlack [24], proposing a number of velocity and Reynolds shear stress distributions which are valid either in the inner or the outer flow regions.

In spite of the above significant efforts, further research concerns the scaling laws and their appropriate scaling parameters for the mean velocity distribution and the momentum transport, and their dependence on flow geometry and dimensionless numbers such as the Reynolds number is still progressing. Therefore, the primary purpose of the present work is to extend the authors previous studies, with particular attention being given to the turbulent momentum transport and the kinetic energy production in two-dimensional fully developed turbulent plane-channel flows. Utilizing the general form of the mean momentum equation for two-dimensional fully developed turbulent flows, the distribution of both quantities are deduced. A Reynolds stress function proposed by Panton [21,22] for the turbulent momentum transport was employed, representing the authors' data well when an appropriate value for the von Kármán constant, i.e., $\kappa = 0.37$, obtained by Zanoun [25] for channel flow is substituted into its functional relationship.

The main sections of the present paper are summarized as follows. Section 2 outlines the main governing equations, utilizing Panton's stress function to treat the turbulent momentum transport and the kinetic energy production in plane-channel flows. The normalized momentum transport and the kinetic energy production data are presented in Section 3 in addition to some normalized mean velocity profiles. This section presents the

* Corresponding author.
E-mail address: f.durst@fmp-technology.com (F. Durst).

0017-9310/$ - see front matter © 2009 Elsevier Ltd. All rights reserved.
doi:10.1016/j.ijheatmasstransfer.2009.03.046

Nomenclature

B, C	constants
g	gravitational acceleration/Panton function
h	channel half height
ℓ_c	viscous length scale
p	pressure
P	turbulent kinetic energy production
U_i	streamwise velocity component
U_j	normalwise velocity component
u'_1	streamwise velocity fluctuation
u'_2	normalwise velocity fluctuation
u_c	characteristic velocity scale
u_τ	wall friction velocity

Greek letters

ρ	fluid density
μ	dynamic viscosity
ν	kinematic viscosity
κ	von Kármán constant
τ_w	mean wall shear stress
η	normalized wall distance

Superscript

+	nondimensional quantity/in wall units

Dimensionless numbers

Re	Reynolds number
R^+	Kármán number

experimental data over a wide range of Reynolds number compared with the current theoretical analysis, pointing out some similarities and differences between the ducted, i.e., channel and pipe, and the boundary layer flows. Section 4 summarizes the outcome of the present study with some concluding remarks. This work contributes hence to a problem once tackled in Prof. Spalding's[1] research work since he made a nice contribution to the formulation of the law of the wall.

2. The governing equations

When the time-averaged Navier–Stokes equations, i.e., the Reynolds-averaged equations,

$$\frac{\partial}{\partial x_i}\left[\rho\overline{U_i U_j} - \left(-\rho\overline{u'_i u'_j} + \overline{\tau_{ij}}\right)\right] = -\frac{\partial p}{\partial x_j} + \rho g_j, \tag{1}$$

are adapted to two-dimensional fully developed turbulent plane-channel flows, the following equation results:

$$-\rho\overline{u'_1 u'_2} + \mu\frac{d\overline{U}}{dy} = \rho u_\tau^2\left(1 - \frac{y}{h}\right). \tag{2}$$

The normalization of all terms in Eq. (2) with the following wall characteristic velocity and length scale:

$$u_c = u_\tau = \sqrt{\tau_w/\rho}, \quad l_c = \nu/u_\tau, \tag{3}$$

results in the following normalized form for the mean momentum equation:

$$-\overline{u'_1 u'_2}^+ + \frac{d\overline{U}^+}{dy^+} = 1 - \eta, \tag{4}$$

where $\eta = y^+/R^+$ is a notation for the normalized wall distance and R^+ is defined as $R^+ = u_\tau h/\nu$, recently, called the Kármán number. The quantity h represents the channel half-height and ν is the kinematic viscosity of the flowing fluid. When the Kármán number tends to infinity, i.e., $R^+ \to \infty$, Eq. (4) is simplified, in terms of wall units, to represent the flow in the wall layer as follows:

$$-\overline{u'_1 u'_2}^+ = 1 - \frac{d\overline{U}^+}{dy^+}, \tag{5}$$

where the viscous shear stress effect cannot be neglected, see Fig. 1.

In the core region $(d\overline{U}^+/dy^+) \ll 1$, hence Eq. (4) written in the outer variables reads as

$$-\overline{u'_1 u'_2}^+ = 1 - \eta. \tag{6}$$

There have been various attempts to match the above inner [Eq. (5)] and outer [Eq. (6)] regions of the flow; see, e.g., [26,20–22]. Panton [21,22] proposed the following Reynolds stress function for two-dimensional turbulent shear flows:

$$g(y^+) = \frac{2}{\pi}\arctan\left(\frac{2\kappa y^+}{\pi}\right)\left[1 - \exp\left(-\frac{y^+}{C^+}\right)\right]^2, \tag{7}$$

where C^+ is a constant that was recommended by Panton [21] to have a value of 7.8 for $\kappa = 0.41$, and recently, 6.2 or 6.78 for $\kappa = 0.37$, see [25] and [22], respectively. Eq. (7) was found to be valid for all values of y^+ and it permits the prediction of the turbulent momentum transport for any Reynolds number as follows:

$$-\overline{u'_1 u'_2}^+ = g(y^+) - \eta, \quad 0 \leqslant \eta \leqslant 1. \tag{8}$$

The way in which relationship Eq. (7) was derived satisfies assumptions to reproduce both Eqs. (5) and (6), see [21]. It was observed also that Eq. (7) has the following general characteristics:

1. It is a smooth function and increases monotonically with increasing the wall distance. It is differentiable with respect to y^+ and is defined in the following interval:

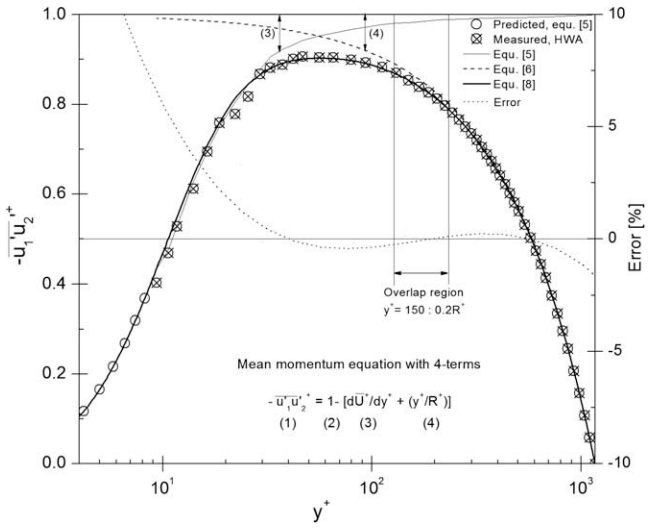

Fig. 1. Magnitude of the four terms in the mean momentum equation, Eq. (4), in two-dimensional fully developed turbulent plane-channel flow for $R^+ = 1167$.

[1] D.B. Spalding, A single formula for the law of the wall, ASME J. Appl. Mech. 83 (1961) 455–458.

$$g(y^+) \in [0,1]. \tag{9}$$

2. It has an asymptotic behavior for $y^+ \to \infty$, to yield

$$g(y^+)|_{(y^+\to\infty)} = 1. \tag{10}$$

3. It has a bounded value for $y^+ \to 0$, i.e., $g(y^+)|_{(y^+\to 0)} = 0$ and, from its definition, one can see that the following relationship holds:

$$\frac{\partial g(y^+)}{\partial y^+}|_{(y^+\to 0)} = 0, \quad \frac{\partial g(y^+)}{\partial y^+}|_{(y^+\to\infty)} = 0. \tag{11}$$

2.1. Turbulent momentum transport and its peak position

One property of interest for the fully developed two-dimensional turbulent channel flows is the peak value of the turbulent momentum transport (i.e., $-\overline{u_1' u_2'}^+_{max}$) which as well as its position is often discussed in the literature. From Eq. (6), one can see that

$$-\overline{u_1' u_2'}^+|_{R^+\to\infty} = 1, \quad \eta \ll 1, \tag{12}$$

which can be obtained also from Eq. (8) for the corresponding positions $y^+ > 1$ and $\eta \ll 1$.

Panton's correlation could also be employed to yield information about the peak and its location of the distribution of $-\rho\overline{u_1' u_2'}$. From Eq. (8) one can write

$$\frac{d}{dy^+}\left(-\overline{u_1' u_2'}^+\right) = \frac{d}{dy^+} g(y^+) - \frac{1}{R^+} \tag{13}$$

to obtain a relationship at which the peak turbulent momentum transport occurs, i.e., for $d\left(-\overline{u_1' u_2'}^+_{max}\right)/dy^+ = 0$ Eq. (13) reduced to

$$\frac{d}{dy^+} g(y^+) = \frac{1}{R^+}, \tag{14}$$

where the differentiation of $g(y^+)$ reads as

$$\frac{d}{dy^+} g(y^+) = 4\left(1 - e^{(-y^+/C^+)}\right)\left[k\frac{1 - e^{(-y^+/C^+)}}{\pi^2 + 4k^2 y^{+2}} + \frac{e^{(-y^+/C^+)}}{\pi C^+}\arctan\left(\frac{2ky^+}{\pi}\right)\right]. \tag{15}$$

Solving Eq. (15) in connection with Eq. (14), numerically, provides the location of the peak $-\overline{u_1' u_2'}^+$ for different Kármán numbers (see Fig. 7).

An alternative scenario to locate the position of the peak of $-\overline{u_1' u_2'}^+$ is to utilize the logarithmic velocity profile, $\overline{U}^+ = 1/\kappa \ln(y^+) + B$, coupled with the mean momentum equation [i.e., Eq. (4)], resulting in another expression for the location of $-\overline{u_1' u_2'}^+_{max}$:

$$y^+|_{-\overline{u_1' u_2'}^+_{max}} = \sqrt{\frac{R^+}{\kappa}}. \tag{16}$$

In addition, based on a variety of data sources, Sreenivasan [27] proposed the following relation for locating the peak $-\overline{u_1' u_2'}^+_{max}$:

$$y^+|_{-\overline{u_1' u_2'}^+_{max}} = 2\sqrt{R^+}. \tag{17}$$

Further processing of the mean momentum equation connected with the logarithmic velocity profile results in the peak value of $-\overline{u_1' u_2'}^+$:

$$-\overline{u_1' u_2'}^+_{max} = 1 - \frac{2}{\sqrt{\kappa R^+}} \;\Rightarrow\; -\overline{u_1' u_2'}^+_{max}|_{R^+\to\infty} = 1. \tag{18}$$

Both Eqs. (16) and (18) clearly indicate a direct dependence of the peak position and the peak value of $-\overline{u_1' u_2'}^+$ on both the von Kármán constant, κ, and the Kármán number, R^+.

2.2. Turbulent kinetic energy production and its peak position

In wall-bounded turbulent shear flows, both the viscous and the turbulent momentum transport terms in Eq. (4), i.e., $(d\overline{U}^+/dy^+)$, and $(-\overline{u_1' u_2'}^+)$, respectively, contribute to the turbulent energy production. Hence the distribution of the turbulent kinetic energy production can be calculated as follows:

$$P^+ = -\overline{u_1' u_2'}^+ \frac{d\overline{U}^+}{dy^+}, \tag{19}$$

and, by introducing the definition of $-\overline{u_1' u_2'}^+$ from Eq. (4) into Eq. (19), the turbulent kinetic energy production can be rewritten as follows:

$$P^+ = -\left(\frac{d\overline{U}^+}{dy^+}\right)^2 + \frac{d\overline{U}^+}{dy^+} - \eta\frac{d\overline{U}^+}{dy^+}. \tag{20}$$

At the point where the viscous and the turbulent shear stresses are equal, i.e., $d\overline{U}^+/dy^+ = -\overline{u_1' u_2'}^+$, Eq. (4) turns to read as

$$\frac{d\overline{U}^+}{dy^+} = \frac{1}{2}[1 - \eta]. \tag{21}$$

Hence, Eq. (20) can be rewritten as

$$P^+ = \left[\frac{1}{2}(1 - \eta)\right]^2. \tag{22}$$

For high enough Kármán number, $\eta \to 0$, therefore one obtains

$$P^+|_{\eta\to 0} = \frac{1}{4}. \tag{23}$$

Alternatively, for the limit of $R^+ \to \infty$, one can see from Eq. (4) that

$$\frac{d\overline{U}^+}{dy^+} = \left[1 - \left(-\overline{u_1' u_2'}^+\right)\right], \tag{24}$$

and in the overlap region, i.e., $y^+ \gg 1$, for high Reynolds numbers the turbulent momentum transport is equivalent to the stress function correlation [Eq. (7)], i.e., $-\overline{u_1' u_2'}^+ \approx g(y^+)$; see [21]. Hence, the turbulent kinetic energy production can be reconstructed as a function of the stress function correlation $g(y^+)$ as follows:

$$P^+|_{(R^+\to\infty)} = g(y^+)[1 - g(y^+)]. \tag{25}$$

Since $g(y^+) \in (0,1)$, it follows that an inflection point exists at $g(y^+)|_{P^+_{max}} = 1/2$, corresponding to the position $y^+_{P_{max}}$ at which the peak turbulent kinetic energy production, i.e., $P^+_{max} = 0.25$, occurs. Moreover, the location of the peak kinetic energy production, $y^+_{P^+_{max}}$, can be obtained by the numerical solution of the following equation that resulted from differentiating equation (25):

$$\tan\left\{\frac{\pi}{4}\left[1 - \exp\left(-\frac{y^+_{P^+_{max}}}{C^+}\right)\right]^{-2}\right\} = \frac{2\kappa y^+_{P^+_{max}}}{\pi}. \tag{26}$$

3. Experimental verification and discussion of results

One of the primary purposes of the present work is to extend previous studies of the authors' results obtained with particular attention being given here to the distributions of the viscous and the turbulent momentum transports and the turbulent kinetic energy production in two-dimensional fully developed turbulent channel flows. Different complementary measuring techniques were utilized [25], and supported by the numerical results of Moser et al. [6] to yield reliable information about the turbulent properties of plane-channel flows.

3.1. Viscous and turbulent momentum transport

In Fig. 2, the turbulent momentum transport data deduced from the mean momentum Eq. (5) are compared with the predicted turbulent momentum transport using the stress correlation function,

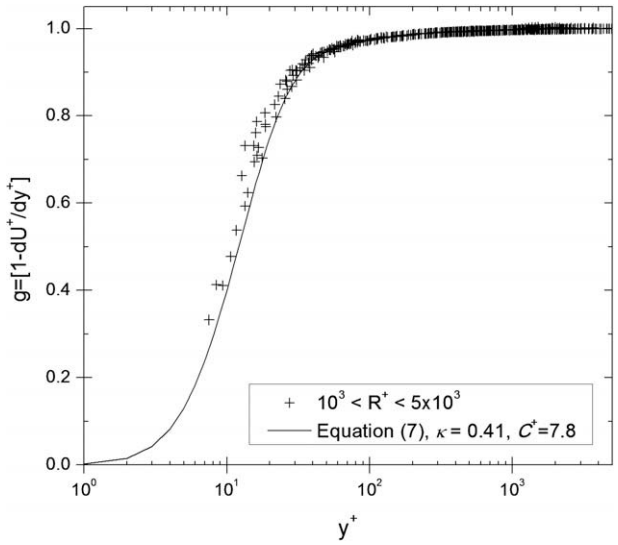

Fig. 2. The computed Reynolds shear stress distributions versus the wall distance over a wide range of Reynolds number compared with Panton stress function [Eq. (7)] in the channel flow.

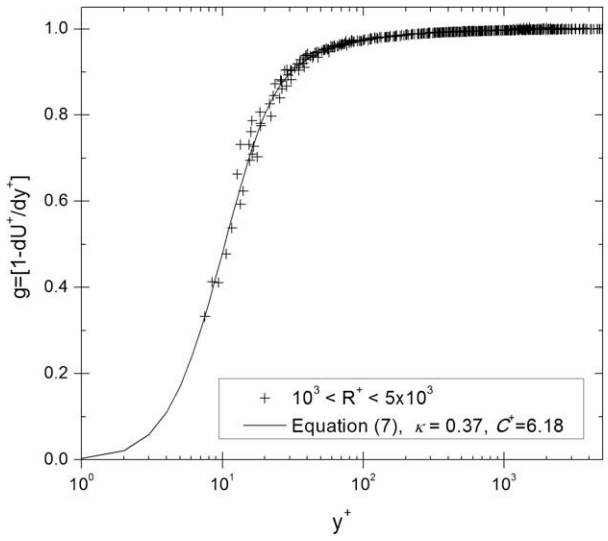

Fig. 4. The computed Reynolds shear stress distributions in the wall layer over a wide range of Reynolds number compared with Panton stress function [Eq. (7)] utilizing the new constants $\kappa = 0.37$ and $C^+ = 6.18$ in the channel flow.

i.e., Eq. (7). The comparison shows good agreement away from the wall, but less agreement in the wall region, i.e., $y^+ < 50$. A possible reason for this disagreement close to the wall is that the value of the constant $C^+ = 7.8$ proposed by Panton [21], based on different sets of data extracted from the literature, was not appropriate. By looking at Panton's [21] paper, a wide scatter among the experimental data was observed because of inaccuracies in both the wall skin friction data and the wall distance measurements. Another reason for the scatter of the data might be attributed to the low Reynolds number effect that resulted in higher values for both constants of the logarithmic velocity profile, i.e., $\kappa = 0.41$ and $B = 5$, and consequently leading to higher value of the Panton's constant (C^+). Hence an accurate estimation for the constant C^+ of Panton's stress function was of prime importance based on the new value for the von Kármán constant, i.e., $\kappa = 0.37$, obtained for channel flow [25]. The computed value of C^+ for different Reynolds numbers does not show in Fig. 3 a clear dependence on the Kármán number. Using the least-squares curve fit for the data presented in Fig. 3, a better value for the constant C^+ was found to be 6.18, see also [25,22]. The stress function of Panton [Eq. (7)] was then re-evaluated with the $\kappa = 0.37$ and $C^+ = 6.18$, resulting in better agreement with both the present computed and predicted turbulent momentum transports for high Reynolds number in Fig. 4.

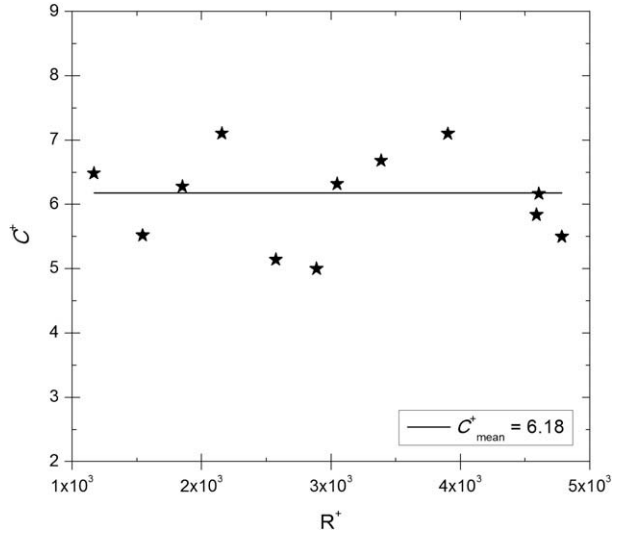

Fig. 3. The Reynolds number effect on Panton's constant C^+ of the Reynolds stress function [i.e., Eq. (7)] in the channel flow.

Based on the structure of the mean momentum equation, the four-layer description of the wall-bounded shear flows is well described and accepted in the fluid mechanics community [3], i.e.,

- laminar sublayer $y^+ \leqslant 5$,
- buffer layer $5 < y^+ \leqslant 30$,
- logarithmic layer $30 < y^+ \leqslant 0.15$ or $0.2R^+$,
- core region $y^+ > 0.15$ or $0.2R^+$.

However, the inner limit of the logarithmic layer was found to be $y^+ = 150$ for the channel flow and the layer for $30 \leqslant y^+ \leqslant 150$ was found to behave in a power manner [28] or called a meso layer [23]. Wei et al. [3] adapted the four-layer description to turbulent wall shear flows, revealing some important issues with the Kármán number scaling properties of the mean momentum balance in both the channel and pipe flows. The momentum transport in each of the four different layers is conducted either by the viscous shear stress, $\mu d\overline{U}/dy$, or by the Reynolds shear stress, $-\rho\overline{u_1'u_2'}$. The viscous shear stress contributes considerably to shearing the flow, mainly, quite close to the wall, and therefore it was observed that $d\overline{U}^+/dy^+ \ll -\overline{u_1'u_2'}^+$ over a large part of the flow, i.e., $y^+ > 100$. However, having a precise distribution of the viscous shear stress in the different wall layers helps in investigating the effect of the Reynolds number on the wall-bounded shear flows no matter how high R^+ is. Eq. (2) underlines a direct relationship between the gradient of the mean velocity distribution, i.e., the viscous shear stress, and the turbulent momentum transport. Hence it forms a basis to obtain information about $-\rho\overline{u_1'u_2'}$, in principle, from simple gradient measurements of both the mean velocity and pressure along the channel test section. On the other hand, earlier attempts have been made either to model or to measure simultaneously the streamwise and normal fluctuations to obtain $-\rho\overline{u_1'u_2'}$. Gad-el-Hak and Brandyopadhyay [15] concluded that the directly measured turbulence shear stress is on average 10% smaller than the theoretical distribution deduced from the momentum balance and the mean flow data, in agreement with Akinlade [29] who found ±11% uncertainty in estimating the

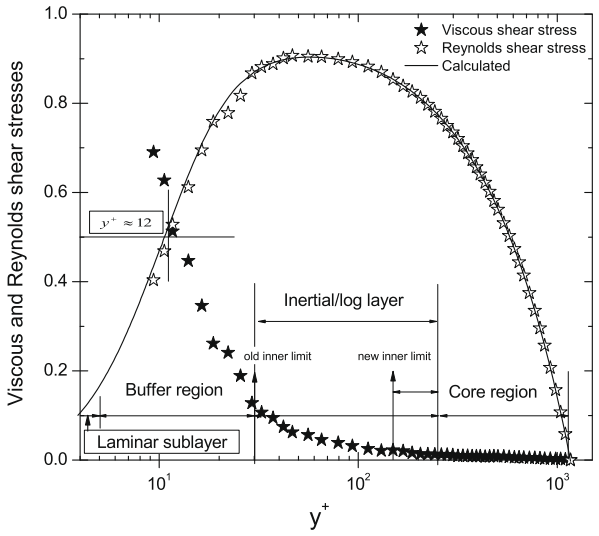

Fig. 5. The normalized viscous and Reynolds shear stresses versus the normalized wall distance in the channel flow for $R^+ = 1167$.

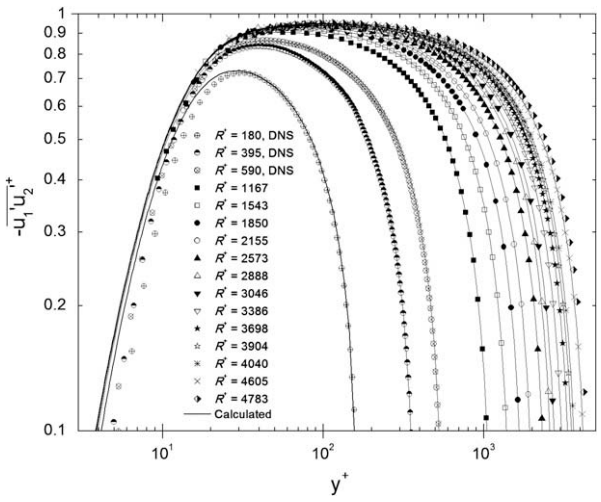

Fig. 6. Distributions of the present Reynolds shear stress over a wide range of Reynolds number compared with the predicted Reynolds shear stress using Panton stress function [Eq. (7)] in the channel flow for $\kappa = 0.37$ and $C^+ = 6.18$.

Reynolds shear stress from the dirtect measurements, see also [30]. Laufer [9] observed also that the total shearing stress obtained from the direct fluctuations measurements was approximately 20% lower than that the computed values from the mean velocity and the mean pressure gradient measurements. The uncertainity in the direct measurements of the Reynolds shear stress arises from the difficulity of carrying out simultaneous measurements of both the streamwise and the normal velocity fluctuations with adequate resolution, particularly, close to the wall, i.e., $y^+ \leqslant 30$ (i.e., $y \leqslant 500$ μm in the present study). This part of the present study therefore reviews some aspects on both the viscous and the turbulent momentum transports distributions in the fully developed two-dimensional plane-channel flows.

The viscous shear stress was obtained directly from the gradient of the mean velocity distribution ($d\overline{U}/dy$), however, the turbulent momentum transport distribution was computed using the mean momentum equation [i.e., Eq. (2)] through the mean velocity gradient and the streamwise mean pressure gradient. The data were normalized with the wall friction velocity, u_τ, obtained either from measurements of the mean pressure gradient or the oil film interferometry [25]. A selected sample of the normalized viscous and turbulent momentum transport is presented in a semi-logarithmic plot in Fig. 5. Closer inspection of the distribution of the viscous and the turbulent shear stresses presented in Fig. 5 demonstrates only three distinguished layers of the channel flow since no data were available for $y^+ \leqslant 5$. The data are presented in a semi-logarithmic plot to show clearly the importance of the thin region, relative to the rest of the total shear layer, close to the wall. This thin layer is composed of two subregions, namely, a viscous/laminar sublayer and the buffer region. In spite of the fact that there is no currently available data for $y^+ \leqslant 5$, it could be supported by the numerical data of Moser et al. [6] as well as the analysis of the RANS equations. Although the viscous term ($d\overline{U}^+/dy^+$) seems to play a negligible role away from the wall, i.e., $y^+ \gg 1$, as can be seen from the figure, however, still has a considerable importance for describing the entire flow field [25]. From Fig. 5, it was also observed that the Reynolds stress is equal to the viscous stress at $y^+ \approx 12$ where the maximum value of the turbulent energy production, $-\overline{u_1'u_2'}(d\overline{U}/dy)|_{max}$, occurs as will be shown later. The near-wall layer is then followed by a region of quasi-constant Reynolds shear stress, see Fig. 6 for more clarity, for the cases of higher Reynolds numbers which extends from $y^+ = 30$ (the old inner limit of the log layer) or from $y^+ = 150$ (the new inner limit of the log layer) to $y^+ = 0.2R^+$ where the momentum transport is mainly accomplished by turbulence. Thereafter, an outer layer, i.e., core region, exists which is characterized by diminishing turbulent shear stress, reaching zero at the channel centerline.

Data of the turbulent momentum transport ($-\overline{u_1'u_2'}^+$) are presented in Fig. 6 over a wide range of Reynolds number, $180 \leqslant R^+ \leqslant 4783$, including three cases from the DNS, Moser et al. [6]. Fig. 6 is a log-log plot that permits closer inspection for the effect of the Reynolds number on the turbulent momentum transport, particularly in the wall region. As can be seen, good collapse of the data was obtained, indicating Reynolds number independence close to the wall, i.e., $y^+ < 100$, for $R^+ \geqslant 2 \times 10^3$. On the other hand, scaling the data with the wall variables do not collapse the $-\overline{u_1'u_2'}^+$ in the core region. For high enough Reynolds numbers, i.e., $R^+ \geqslant 2 \times 10^3$, the $-\overline{u_1'u_2'}^+$ approaches a maximum value outside the viscous sublayer and shows approximately a constant behavior along the overlap region as the Reynolds number increases. Thereafter, the $-\overline{u_1'u_2'}^+$ decreases in the channel core region because of the streamwise mean pressure gradient.

To further proceed, the distance from the wall in the wall viscous units, where the peak $-\overline{u_1'u_2'}^+|_{y^+_{max}}$ occurs, is illustrated in Fig. 7. Fig. 7 shows good agreement among the authors' experimental results and data obtained from Eqs. (15)–(17). It is clear from Fig. 7 that the location where the maximum value of $-\overline{u_1'u_2'}^+$ occurs depends strongly on the Kármán number. It moves away from the wall as the Kármán number increases. Panton [21] interpreted the movement of the location of the peak value of $-\overline{u_1'u_2'}^+$ as a simple consequence of the inner and outer layers mixing of different sizes as R^+ increases. However for the current range of the Reynolds number, it was observed that the location of the peak $-\overline{u_1'u_2'}^+|_{y^+_{max}}$ lies outside the log-law layer, considering the inner limit $y^+ = 150$ of the log range, reflecting some lack of the assumptions that resulted in Eq. 16. The magnitude of the peak of the turbulent momentum transport, $-\overline{u_1'u_2'}^+|_{y^+_{max}}$, versus the Kármán number, R^+, is provided in Fig. 8. It can be seen that $-\overline{u_1'u_2'}^+|_{y^+_{max}}$ increases with increasing the Reynolds number and there is good agreement between the authors' results deduced from the mean momentum equation and the data extracted from Panton's relation. It is also believed that as the Reynolds number increases, the peak value of $-\overline{u_1'u_2'}^+$ continues to increase, but the limiting value is unity as the Reynolds number, asymptotically,

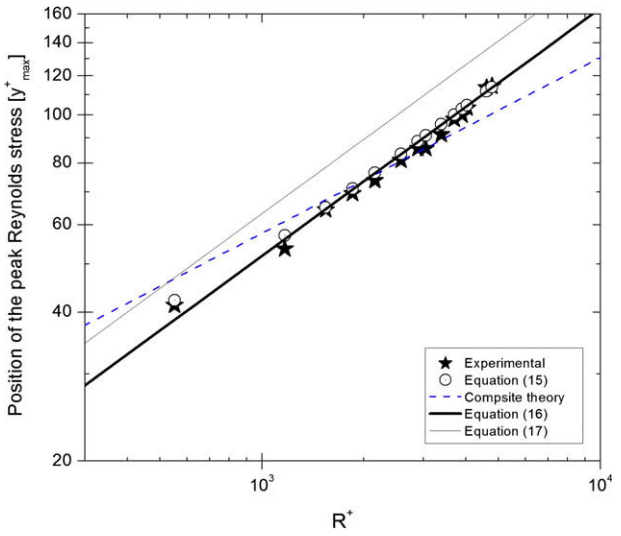

Fig. 7. Location of the peak Reynolds shear stress versus the Kármán number in the channel flow.

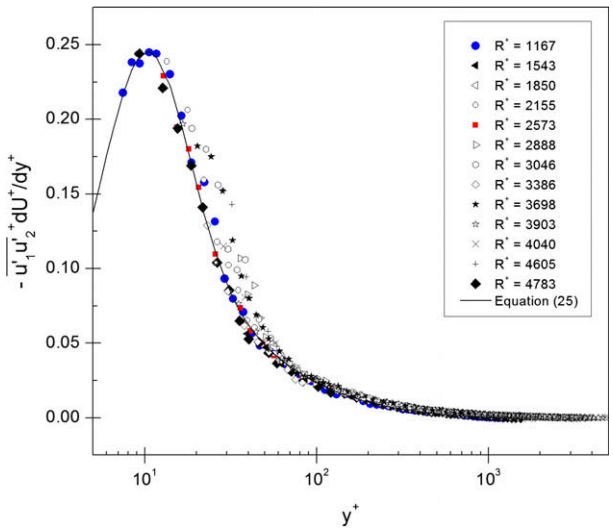

Fig. 9. The normalized turbulent kinetic energy production distributions versus the normalized wall distance in the channel flow.

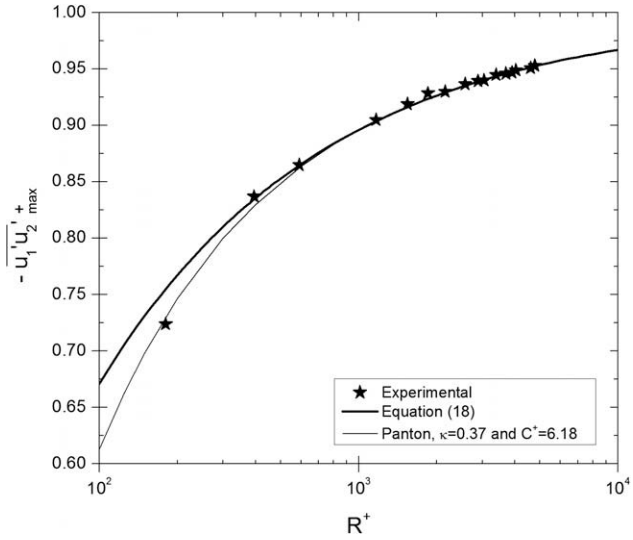

Fig. 8. Behavior of the peak Reynolds shear stress versus the Kármán number in the channel flow.

reaches infinity that was also deduced in section 2.1 [see Eqs. (12 and 18)].

3.2. Turbulent kinetic energy production

The Reynolds number effect on the distribution of the turbulent kinetic energy production in channel flows is presented in Fig. 9. The turbulent kinetic energy production was calculated via the turbulent momentum transport $(-\rho\overline{u_1'u_2'})$ and the mean velocity gradient $(d\overline{U}/dy)$. The results were normalized with the wall variables (i.e., u_τ and $l_c = \nu/u_\tau$) and then presented in dimensionless form versus the normalized wall distance, y^+. Fig. 9 shows good collapse of the turbulent kinetic energy production results and therefore a Reynolds number independence can be concluded for high enough Kármán number, i.e., $R^+ > 10^3$. In addition, a peak value was observed at a fixed distance from the wall, i.e., $y^+ \approx 12$, which agrees well with Wei and Willmarth [30], Gad-el-Hak and Bandyopadhyay [15], Sahay and Sreenivasan [17] and more recently with Laadhari [4]. Moreover, good agreement was obtained between the present experimental results and the prediction of the turbulent kinetic energy production utilizing Eq. (25). The position of the maximum kinetic energy production was found to coincide with the wall-normal position at which the turbulent and the viscous shear stresses are equal, see Fig. 5. The peak value of the turbulent kinetic energy production as can be seen from Fig. 9 was found to be approximately 0.25, confirming Eq. (23).

3.3. Channel versus pipe and boundary layer flows

There are some remarkable flow similarities and differences between the ducted, i.e., rectangular channel and/or circular pipe, and boundary layer of zero pressure gradient turbulent shear flows, see; e.g., Sreenivasan [27]. These are two classes of shear flows that are fundamentally different in a sense that channel and pipe flows are just fully developed while boundary layers are developing flows. However, a comparison among them can be made, for instance, from Fig. 10 one can observe that the mecha-

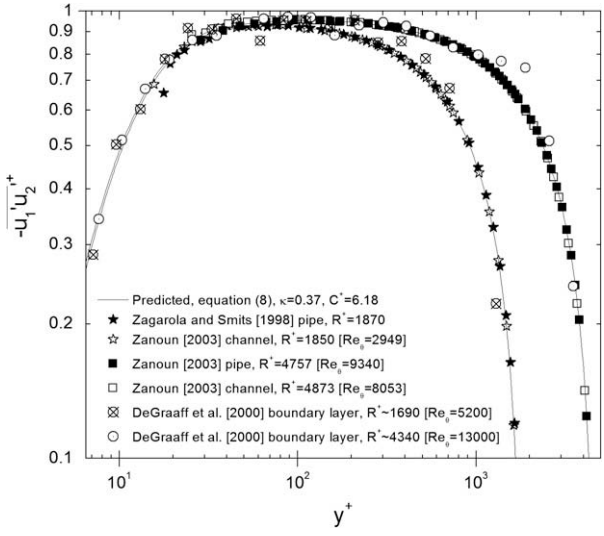

Fig. 10. The distributions of the Reynolds shear stress in the channel and the pipe flows for almost two identical Reynolds numbers compared with the flat plate turbulent boundary layer and the predicted Reynolds shear stress using Panton stress relation.

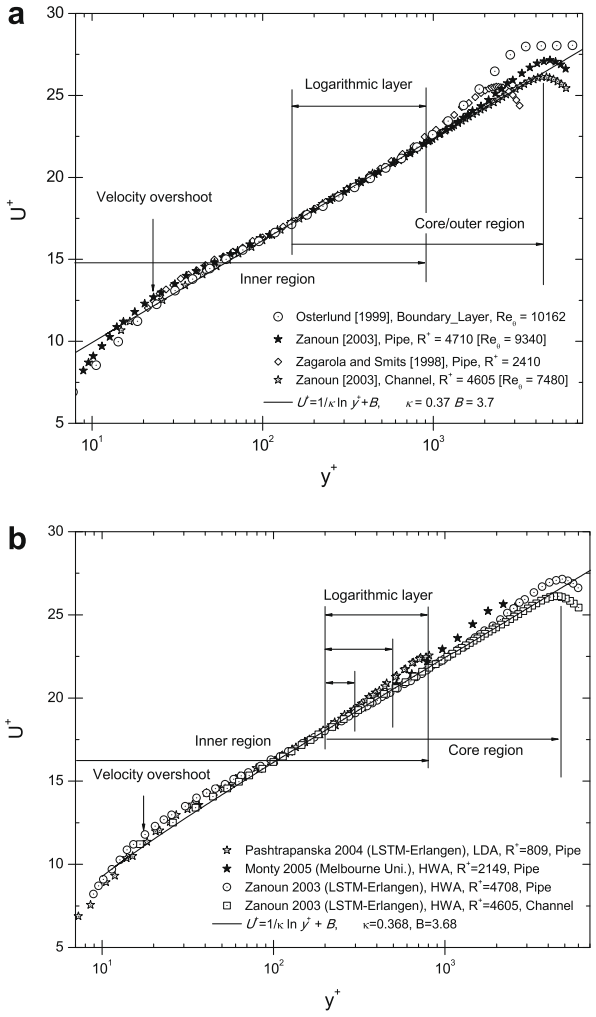

Fig. 11. The present mean velocity distribution for different Reynolds numbers in the channel, the pipe and the flat plate turbulent boundary layer flows compared with the logarithmic velocity profile.

nism of the turbulent momentum transport in these two classes of shear flows is quite similar in spite of the geometrical differences between them. For both types of flows, the distribution of the turbulent momentum transport shown in Fig. 10 for almost the same Kármán numbers was found to be similar in the viscous and the logarithmic layers, extending to the core/outer region, in contrast to differences observed in the mean velocity distributions either within the viscous sublayer or in the core/outer region, see Fig. 11. In the channel flow, particularly, at low Reynolds number, it was speculated by Wei and Willmarth [30] that the inner-region structure from the opposing walls interacted where a constant interchange of counter-rotating vorticity between the two inner regions exist due to bursting, see also [14]. A similar phenomenon in the turbulent boundary layer flow does not exist [31] because there is only one wall and the pipe flow is even more complex, see Wei and Willmorth [30] for more details.

Comparison of the present mean velocity profiles in the channel with those of Zagarola and Smits [32], Monty [33], Pashtrapansaka [34] and Zanoun [25] are presented in Fig. 11b for different Reynolds numbers. However, the comparison made in Fig. 11a was at similar Reynolds numbers to examine the details of the differences between these two ducted flows versus a selected case from the zero pressure gradient flat plate boundary layer data of Österlund [35]. It appears that the superpipe results of Zagarola and Smits [32] show good agreement with the channel flow results in the overlap region, but there is less agreement in both the core region and within the viscous sublayer. It is worth noting that the cases presented either in Fig. 10 or Fig. 11 from the data of Zagarola and Smits [32] are near the lower end of their Reynolds number range; however, the parameters of the logarithmic velocity profile ($\kappa = 0.436$ and $B = 6.13$) reported by them were derived from their entire range of their Reynolds numbers. More recently, Perry et al. [36] advanced a different interpretation of the superpipe data, concluding that a more appropriate representation of the superpipe results leads to values of $\kappa = 0.39$ and $B = 4.0$ for the logarithmic law parameters. Their alternative interpretation was based on evidence extracted from the data of Zagarola and Smits [32] that for a substantial range of higher Reynolds numbers, the flow in the superpipe experiments was transitionally rough. The same agreement and conclusion can also be made when the present channel data are compared with the pipe flow data of Zanoun [25], Monty [33], Pashtrapansaka [34]. Careful examination of the results in Fig. 11 reveals also an often forgotten aspect of the flow in the channel when contrasted with the pipe flow. The deviation from the logarithmic law in the core region of the channel flow is considerably less than that for the flow through pipes. This suggests that the logarithmic law may be valid much closer to the line of symmetry of the flow in the case of the channel. This observation was made by Prandtl [37], Wei and Willmarth [30] and Gad-el-Hak and Bandyopadhyay [15] many years ago, but is often forgotten in the turbulence literature. The fact that the deviation from the overlap region in the outer flow of the pipe is larger than that for the channel may also be contrasted with the even larger deviation observed in the case of the boundary layer, i.e., the wake component. This result is counter-intuitive when one compares the three cases since, based on the relative size (volume) of the outer flow, with respect to the vorticity-generating wall surface, the channel may be assumed to fall between the boundary layer and the pipe. The fact that the deviation in the outer flow of the pipe falls between those of the other two is inconsistent with the above argument. This result suggests that the channel flow may have the least influence of the core flow on the wall region in these wall-bounded turbulent shear flows, motivating for further research in connection with clarifying the character of the outer layer (i.e., wake region) among the three types of the wall-bounded shear flows.

4. Conclusions

Experimental data for two-dimensional fully developed turbulent plane-channel flow, up to more than twice the highest Reynolds numbers previously available, have been documented based on two independent measurements of the wall shear stress [25], resulting in the following conclusions:

The mean velocity distributions in both the viscous sublayer and the core region show differences among the three wall-bounded shear flows. The outer flow deviation from the logarithmic law is the smallest for the channel with the case of the pipe remaining considerably smaller than the zero pressure gradient boundary layers; these trends reflect the combined effects of flow geometry and pressure gradient. This suggests that the logarithmic law may be valid much closer to the line of symmetry of the flow in the case of the channel flow.

This work permitted also valuable evaluation of the Kármán number, R^+, effect on both the viscous and the turbulent momentum transport and the kinetic energy production. The turbulent momentum transport data seems to scale with the inner wall variables, showing Reynolds number independence close to the wall, i.e., $y^+ < 100$, but only for high enough Kármán number. The

present set of data allowed also an accurate evaluation for Panotn's constant C^+ in his Reynolds stress function [Eq. 7]. It provided an excellent agreement with the authors' measurements when the new coefficients $\kappa = 0.37$ and $C^+ = 6.18$ were utilized. This readily suggests that Panton's correlation can be used to extend the authors' results in two-dimensional fully developed turbulent plane-channel flows.

The mechanism of the turbulent momentum transport in both ducted flows, i.e, the channel and the pipe, and the zero pressure gradient boundary layer flows is fairly similar as Fig. 10 showed. This observation came out in spite of the fact that the curvature of the pipe inner wall makes the flow structure of the inner-region from the different circumferential locations interacts at the center of the pipe, resulting in a different turbulent structure than in the channel as well as in the turbulent boundary layer flows where there is only one wall, see [30,31,38,39].

A Reynolds number independence of the turbulent kinetic energy production was observed for $R^+ > 10^3$ when the data were scaled with the inner wall variables and a peak value of approximately 0.25 was obtained at $y^+ \approx 12$. The position of the peak kinetic energy production was found to coincide with the wall-normal position at which the turbulent and the viscous momentum transports are equal.

Further work, extending the two-dimensional channel flow of high aspect ratio and for higher Reynolds number, at least twice the highest Reynolds number achieved in the present experiments and even higher, with high enough resolution, precise and independent wall skin friction data is needed to further support the present analysis.

Large channel test facility is therefore recommended [1] allowing high Reynolds number measurements with good enough spatial resolution in order to have a better understanding of the physics of wall turbulence in rectangular ducts.

Acknowledgements

The authors acknowledge funds received from LSTM–Erlangen, Friedrich Alexander University, to carry out this work. The major funding was received, however, from the Deutsch Forschungsgemeinschaft through DFG-Contract DU 101/75-1.

References

[1] E.-S. Zanoun, H. Nagib, F. Durst, Refined C_f relation for turbulent channels and consequences for high Re experiments, Fluid Dyn. Res. 41 (2009) 021405, 1–12.
[2] J.P. Monty, J.A. Stewart, R.C. Williams, M.S. Chon, Large-scale features in turbulent pipe and channel flows, J. Fluid Mech. 589 (2007) 147–156.
[3] T. Wei, P. Fifa, J. Klewicki, P. McMurtry, Properties of the mean momentum balance in turbulent boundary layer, pipe and channel flows, J. Fluid Mech. 522 (2005) 303–327.
[4] F. Laadhari, The evolution of maximum turbulent kinetic energy production in a channel flow, J. Phys. Fluids 14 (10) (2002) L65–L68.
[5] M. Fischer, Turbulente wandgebundene Strömungen bei kleinen Reynoldszahlen, Dissertation, Universität Erlangen Nürnberg, 1999.
[6] R.D. Moser, J. Kim, N.N. Mansour, Direct numerical simulation of turbulent channel flow up to $Re_\tau = 590$, J. Phys. Fluids 11 (1999) 943–945.
[7] J. Kim, P. Moin, R. Moser, Turbulence statistics in fully developed channel flow at low Reynolds number, J. Fluid Mech. 177 (1987) 133–166.
[8] A.V. Johansson, P.H. Alfredsson, On the structure of turbulent channel flow, J. Fluid Mech. 122 (1982) 295–314.
[9] J. Laufer, Investigation of turbulent flow in a two-dimensional channel, NACA Report R-1053, NACA Washington, DC, 1951.
[10] G. Comte-Bellot, Turbulent flow between two parallel walls, Ph.D. Thesis (in French), University of Grenoble (in English as ARC 31609), 1963, FM 4102.
[11] J.A. Clark, A study of incompressible turbulent boundary layers in channel flow, ASME J. Basic Eng. 90 (1968) 455–468.
[12] H. Eckelmann, The structure of the viscous sublayer and the adjacent wall region in a turbulent channel flow, J. Fluid Mech. 65 (1974) 439–459.
[13] A.K.M.F. Hussain, W.C. Reynolds, Measurements in fully developed turbulent channel flow, Trans. ASME J. Fluids Eng. 97 (1975) 568–580.
[14] R.B. Dean, P. Bradshaw, Measurements of interacting turbulent shear layers in a duct, J. Fluid Mech. 78 (1976) 641–676.
[15] M. Gad-el-Hak, P.R. Bandyopadhyay, Reynolds number effect on wall-bounded flows, Appl. Mech. Rev. 47 (1994) 307–365.
[16] F. Durst, M. Fischer, J. Jovanovic, h. Kikura, Methods to set up and investigate low Reynolds number, fully developed turbulent plane channel flow, Trans. ASME 120 (1998) 496–503.
[17] A. Sahay, K.R. Sreenivasan, The wall-normal position in pipe and channel flows at which viscous and turbulent shear stresses are equal, J. Phys. Fluids 11 (1999) 3186–3188.
[18] P.A. Monkwetiz, H.M. Nagib, The asymptotic structure of high-Reynolds number boundary layers, IUTAM, 2004.
[19] C.M. Millikan, A critical discussion of turbulent flows in channels and circular tubes, in: Proc. of the 5th Int. Congr. Appl. Mech., Wiley, New York, 1938, pp. 386–392.
[20] N. Afzal, K.S. Yajnik, Analysis of turbulent pipe and channel flows at moderately large Reynolds number, J. Fluid Mech. 61 (1973) 23–31.
[21] R.L. Panton, A Reynolds stress function for wall layers, J. Fluids Eng. 119 (1997) 325–330.
[22] R.L. Panton, Composite asymptotic expansions and scaling wall turbulence, Philos. Trans. Roy. Soc. A 365 (2007) 733–754.
[23] M. Wosnik, L. Castillo, W. George, A theory for turbulent pipe and channel flows, J. Fluid Mech. 421 (2000) 115–145.
[24] M. Oberlack, A unified approach for symmetries in plane parallel turbulent shear flows, J. Fluid Mech. 427 (2001) 299–328.
[25] E.-S. Zanoun, Answers to some open questions in wall-bounded laminar and turbulent shear flows, Ph.D. Thesis, Universität Erlangen Nürnberg, 2003.
[26] H. Tennekes, Outline of a second-order theory of turbulent pipe flow, AIAA J. 6 (1968) 1735.
[27] K.R. Sreenivasan, The turbulent boundary layer, in: M. Gad-el-Hak (Ed.), Frontiers in Experimental Fluid Mechanics, Lecture Notes in Engineering, vol. 46, Springer, Berlin, 1989, pp. 159–209.
[28] E.-S. Zanoun, F. Durst, H. Nagib, Scaling laws for turbulent channel and pipe flows over a wide range of Reynolds number, in: Proc. of the 4th Int. Conf. on Heat Transfer, Fluid Mechanics and Thermodynamics, HEFAT, Cairo, Egypt, 2005.
[29] O.G. Akinlade, Effects of surface roughness on the flow characteristics in a turbulent boundary layer, Ph.D. Thesis, University of Saskatchewan, Saskatoon, 2005.
[30] T. Wei, W.W. Willmarth, Reynolds number effects on the structures of a turbulent channel flow, J. Fluid Mech. 204 (1989) 57–95.
[31] R.A. Antonia, M. Teitel, J. Kim, L.W.B. Browne, Low Reynolds number effects in a fully developed turbulent channel flow, J. Fluid Mech. 2363 (1992) 579–605.
[32] M.V. Zagarola, A.J. Smits, Mean-flow scaling of turbulent flow, J. Fluid Mech. 373 (1998) 33–79.
[33] J.P. Monty, Developments in smooth wall turbulent duct flows, Ph.D. Thesis, University of Melbourne, 2005.
[34] M. Pashtrapanska, Experimentelle Untersuchung der turbulenten Rohrströmungen mit abklingender Drallkomponente, Dissertation, Universität Erlangen Nürnberg, 2004.
[35] J.M. Österlund, A.V. Johansson, H.M. Nagib, M.H. Hites, A note on the overlap region in turbulent boundary layers, J. Phys. Fluids 12 (2000) 1.
[36] A.E. Perry, S. Hafez, M.S. Chong, A possible reinterpretation of the Princeton superpipe data, J. Fluid Mech. 49 (2001) 395–401.
[37] L. Prandtl, Über die ausgebildete Turbulenz, Z. Angew. Math. Mech. 5 (1925) 136–139.
[38] J. Rotta, Experimenteller Beitrag zur Entstehung turbulenter Strömung im Rohr, Ing. Archiv. 24 (1956) 258.
[39] V.C. Patel, M.R. Head, Some observations on skin friction and velocity profiles in fully developed pipe and channel flows, J. Fluid Mech. 38 (1969) 181–201.